



**HAL**  
open science

## The geodetic laser interferometers at Gran Sasso, Italy: recent modifications and correction for local effects.

Antonella Amoruso, Luca Crescentini

► **To cite this version:**

Antonella Amoruso, Luca Crescentini. The geodetic laser interferometers at Gran Sasso, Italy: recent modifications and correction for local effects.. *Journal of Geodynamics*, 2009, 48 (3-5), pp.120. 10.1016/j.jog.2009.09.025 . hal-00594437

**HAL Id: hal-00594437**

**<https://hal.science/hal-00594437>**

Submitted on 20 May 2011

**HAL** is a multi-disciplinary open access archive for the deposit and dissemination of scientific research documents, whether they are published or not. The documents may come from teaching and research institutions in France or abroad, or from public or private research centers.

L'archive ouverte pluridisciplinaire **HAL**, est destinée au dépôt et à la diffusion de documents scientifiques de niveau recherche, publiés ou non, émanant des établissements d'enseignement et de recherche français ou étrangers, des laboratoires publics ou privés.

## Accepted Manuscript

Title: The geodetic laser interferometers at Gran Sasso, Italy: recent modifications and correction for local effects.

Authors: Antonella Amoruso, Luca Crescentini

PII: S0264-3707(09)00092-1  
DOI: doi:10.1016/j.jog.2009.09.025  
Reference: GEOD 919

To appear in: *Journal of Geodynamics*



Please cite this article as: Amoruso, A., Crescentini, L., The geodetic laser interferometers at Gran Sasso, Italy: recent modifications and correction for local effects., *Journal of Geodynamics* (2008), doi:10.1016/j.jog.2009.09.025

This is a PDF file of an unedited manuscript that has been accepted for publication. As a service to our customers we are providing this early version of the manuscript. The manuscript will undergo copyediting, typesetting, and review of the resulting proof before it is published in its final form. Please note that during the production process errors may be discovered which could affect the content, and all legal disclaimers that apply to the journal pertain.

# **The geodetic laser interferometers at Gran Sasso, Italy: recent modifications and correction for local effects.**

**Antonella Amoruso and Luca Crescentini**

**Department of Physics, University of Salerno, Italy**

## **Abstract**

Two laser interferometers for geophysical researches are operating under the Gran Sasso massif, Central Italy, since several years. Their electro-optical set-up has been recently modified with respect to the original version to reduce costs and improve reliability. Output of each interferometer now consists of two quadrature signals, whose Lissajous figure is inverted for changes in length of the 90-m-long baselines. These top-rank instruments give high-quality strain data, but siting effects produce coupling among the different strain components, so that measured strain is not equal to the large-scale Earth strain. We estimate local effects using reference tidal strains and a matrix representation of the relationship between instrument and remote strains. The three coupling coefficient of each interferometer (obtained by best-fitting) are able to reduce differences between observed and predicted tides down to negligible levels.

## **1. Introduction**

Ground displacement - caused by the transit of seismic waves and measured by means of inertial seismometers - has been the main tool to investigate the Earth for more than a century. Main drawbacks of inertial seismometers include rapid decreasing of sensitivity with diminishing frequency of ground oscillations and scarce capability of recording slow transients.

Continuous strain measurements can overcome the above-mentioned drawbacks. The most common techniques for continuous strain measurements are (i) continuous GPS (CGPS) nets, measuring displacement of a set of benchmarks with respect to a reference one (distance between benchmarks is of the order of kilometres), (ii) mechanical borehole dilatometers and strainmeters, (iii) mechanical extensometers, measuring distance changes between two end points by means of wires or bars and suitable transducers, and (iv) laser extensometers, measuring distance changes between two end points by means of optical interferometers, usually Michelson-type ones.

The words “extensometers” and “strainmeters” are often used as synonyms. For an old still-valuable review of items (ii) to (iv) see Agnew (1986).

CGPSs allow monitoring large areas at relatively low cost, but their sensitivity is not high (about  $10^{-6}$ - $10^{-7}$ ). Borehole dilatometers and tensor strainmeters are the most widely used high-sensitivity instruments; tens of such devices are working mainly in the United States, China and Japan. A few observatories are equipped with mechanical extensometers (e. g., Black Forest Observatory, <http://www-gpi.physik.uni-karlsruhe.de/pub/widmer/BFO/> and Moxa Geodynamical Observatory, <http://www.geo.uni-jena.de/Homepage-Moxa-englisch/start.html>, in Germany). Superficial long-baseline (about 1-km long) interferometers have been installed in California (see e.g. <http://pfostrain.ucsd.edu/>), their main disadvantages being the high cost of the vacuum system (generally speaking, in each laser interferometers the laser beam has to propagate in an evacuated environment in order to achieve good signal-to-noise ratios) and the necessity of monitoring end-monument displacements with respect to the bedrock at about 30-m depth (e. g. using optical anchors) because of weathering effects, even in case end monuments are embedded in competent granite.

Few laser interferometers, 20 to 100 meter long, have been installed inside tunnels. Both the oldest, no more working, instruments (e. g. Levine and Hall, 1972; Goultly et al., 1974) and the still working ones (e. g. Crescentini et al., 1997; Buklerskii et al., 1995; Takemoto et al., 2004) have shown excellent behaviour. Their long-term (weeks to years) stability has proved to be better than mechanical extensometers and borehole instruments, sensitivity is higher than CGPS' by orders of magnitude, and they can measure strain even in porous fluid saturated rock. Main drawbacks of underground laser interferometers are costs of tunnel excavation, prevalent use of complex electro-optical set-ups (with possible difficulty in obtaining long continuous records and need for frequent adjustments by qualified personnel) and short (with respect to superficial installations) baselines.

At least in principle, laser strainmeters allow an advanced study of geodynamic phenomena, both local and global, in a spectrum ranging from short period seismic waves to tectonic deformation. Among local phenomena, we can mention single-site measurement of seismic phase velocities (comparison of straingrams and seismograms recorded during the transit of seismic waves provide information on wave characteristics which cannot be derived from observations with either instrument alone; in particular, it is possible to determine the phase velocity of the seismic wave by taking ratio of both records, e. g. Sacks et al., 1976), slow earthquakes (discontinuous, earthquake-like events that release energy over a period much longer than usual earthquakes, e. g. Crescentini et al., 1999; Amoruso et al., 2002), deformation induced by seasonal charging and discharging of the local or regional aquifer. Global phenomena include the study of the free oscillations of the Earth (the capability of strainmeters of observing fundamental toroidal modes is much higher than that of horizontal seismometers, e. g. Park et al., 2008) and strain tides (as regards the diurnal resonance due to the free core nutation, see e. g. Mukai et al., 2004).

In what follows, extensions are expressed as dimensionless strain,  $\Delta/l$ , where  $l$  is instrument length, and  $\Delta l$  is positive for an increase in length. We use the symbol  $n\epsilon$ , nanostrain, for  $\Delta/l = 10^{-9}$ .

## 2. The geodetic laser interferometers at Gran Sasso

Two geodetic interferometers have been installed beside the Gran Sasso Tunnel (10.4 km long) on the highway connecting Rome to Teramo (Central Italy), at about 5 km from the East entrance, and in the vicinity of an underground laboratory for Particle Physics and Astrophysics (INFN – Laboratori Nazionali del Gran Sasso), taking advantage of the galleries that surround the main halls of the laboratory. Such galleries were extended to constitute an isosceles right-angled triangle located more than 250 m aside from the highway, and at least 1100 m under the free surface. The two interferometers are located along the catheti of the triangle, each about 90 m long, and whose azimuths are about N66E and N24W. The former baseline, referred to as BC, is approximately perpendicular to the local direction of the Apennines, and the latter, referred to as BA, is approximately parallel to it (see Figure 1).

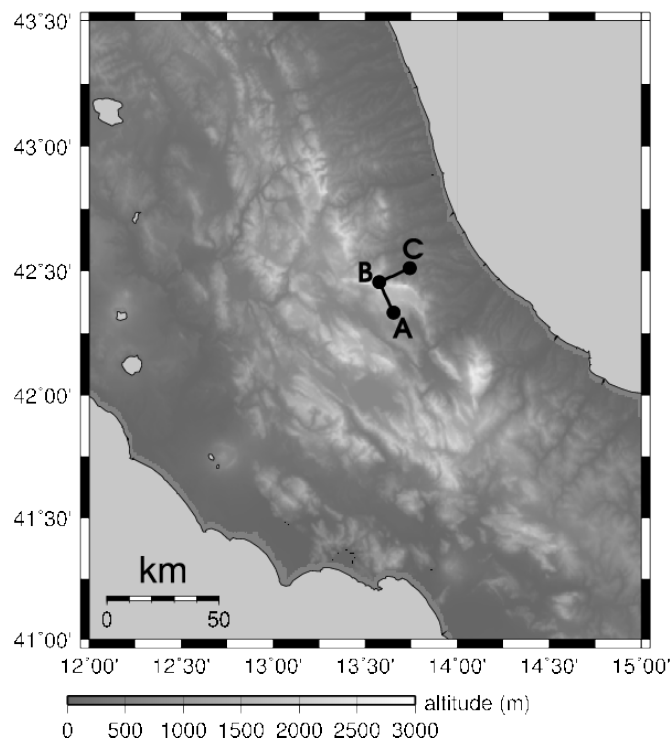


Figure 1. Location and directions of the laser strainmeters operating at Gran Sasso.

The two interferometers have operated since summer 2000. They were developed on the basis of a previous instrument working in the same place from 1994 to 1999 (Crescentini et al. 1997), with some electronic and optical improvements.

Each interferometer is based on the classical unequal-arm Michelson set-up and compares the optical length (i. e. the length expressed in terms of the light wavelength) of a longer measurement arm (90 meters in length) and a shorter fixed reference arm that is 20 cm in length.

Till February 2005 the reference arm included an electro-optical phase modulator, consisting of an optically active crystal whose optical length depends on the electric field it is embedded in. The electric field was dynamically modulated by a feedback loop to stabilize the interference pattern between the laser beams propagating through the reference and measurement arms. The intrinsically small dynamics of the phase modulator had been overcome by changing its optical thickness by one wavelength each time the phase shift is  $+\pi$  or  $-\pi$ . The jumps prevented the interferometers from working for about 50  $\mu$ s. When no jump was involved, the bandwidth reached a few hundred kHz (Crescentini and Renzella, 1991). Voltage applied to the phase modulator was sampled at 800 Hz by a 12-bit digital-to-analog converter. Each datum consisted of two numbers, the former related to the voltage applied to the phase modulator, and the latter related to the number of jumps since the acquisition started. Both sequences of numbers were digitally filtered using a linear non-recursive filter, decimated at 5 Hz, and recorded. Such a configuration allowed recording data at any frequency, after applying a proper low-pass digital filter to the two above mentioned sequences of numbers. This feature of the apparatus was particularly useful in the past, when local storage of huge amount of data was a difficult task, but it requires expensive electro-optical components, a very accurate optical alignment and electronic adjustment, and an occasional careful data pre-analysis to correct for wrong jump counting.

Since February 2005 to May 2006 the experimental set-up underwent major changes (see Figure2) to reduce costs of future installations and improve reliability.

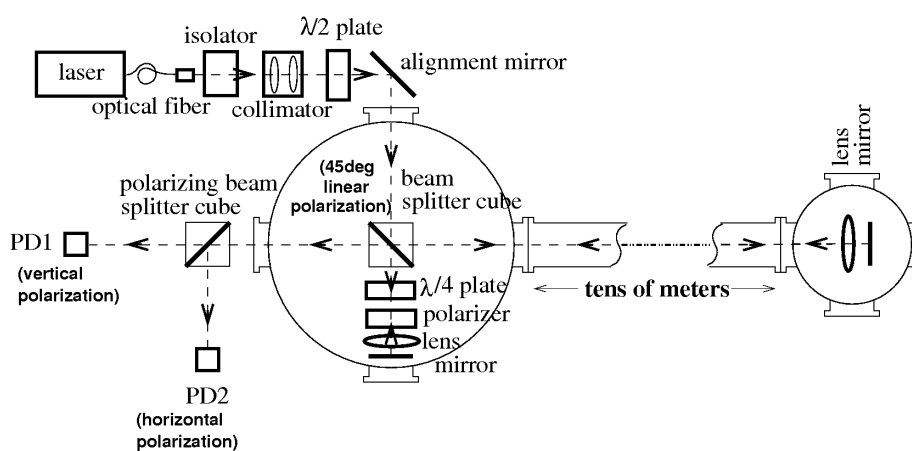


Figure 2. Sketch of the optical set-up of each laser strainmeter (interferometer)

Present electro-optical configuration is much simpler: the reference arm includes only what required to get two quadrature signals at one output for each interferometer (the other output is not used, differently from Crescentini and Amoruso, 1996) i. e. a polarizer and a quarter-wave retarder plate, and external optical components no longer include Faraday rotators. Also the electronics are now much simpler, consisting only in what necessary to measure light intensity at the photodiodes.

As a drawback, phase mismatch (which is proportional to strain) is no longer linearly related to the ADC output, which in turn can not be simply low-passed and decimated before storage. Real time conversion from light intensity to phase (i. e., strain) is not possible, because instabilities of the DC level and amplitude of the interference signal as well as phase lag fluctuations between the quadrature signals ask for a non-linear fit of the Lissajous figure given by few hours of data (see Figure 3). Photodiode outputs are sampled and stored at 600 Hz to avoid artificial mixing of frequencies due to the non-linear dependence of light intensity on phase mismatch. Intensity-to-phase conversion is accomplished on stored signals when needed.

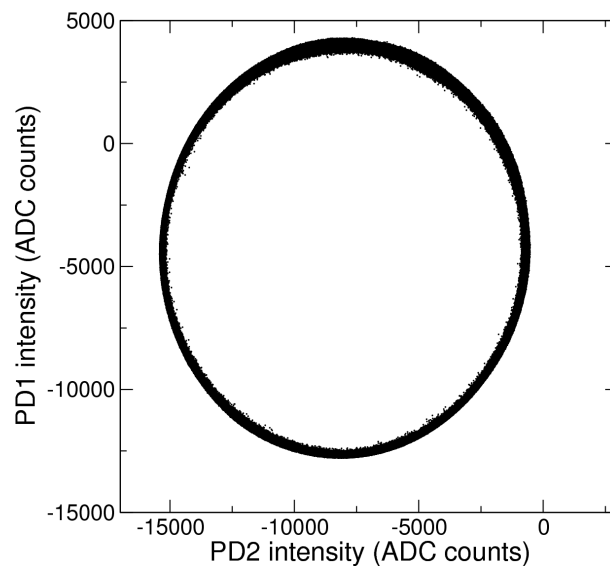


Figure 3. Scatter plot of 3 Msamples recorded by the BA interferometer. A complete round along the ellipse (whose axis lengths and orientations slightly change with time) is due to a baseline-length change by half a wavelength of the laser source (about  $3.5 \text{ n}\epsilon$  in strain).

Two-year data recorded with the new configuration show that changes did not degrade instrumental performances. As an example, Figure 4 shows the power spectral density of 45-day-long detided strain records collected in Autumn 2004 (before instrumental modifications) and 2007 (after instrumental modifications).

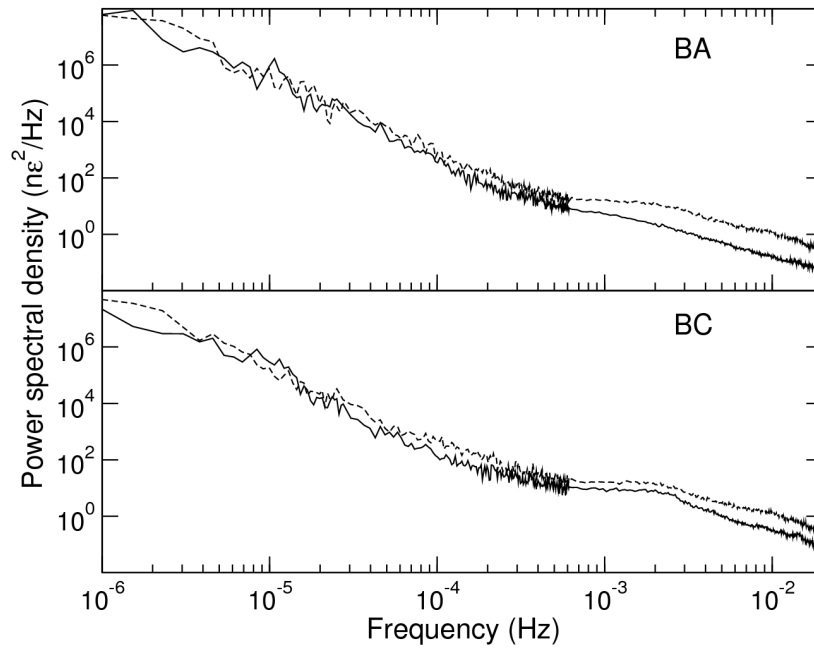


Figure 4. Power spectral density (PSD) of 45-day-long detided strain records collected in Autumn 2004 (dashed lines) and 2007 (solid lines). Top, BA interferometer; bottom, BC interferometer. PSDs at frequencies higher than 0.02 Hz are not shown because of the large variability related to seismic and microseismic activity.

In an unequal-arm Michelson interferometer whose measurement arm is much longer than the reference arm, strain in the measurement arm and fractional changes in wavelength (or frequency) of the laser light are numerically equivalent. This means that a change in the laser light wavenumber can not be distinguished from a change in the length of the measurement arm. If  $\Delta l/l$  is the apparent difference in optical length between the measurement and reference arm, and  $f$  is the laser light frequency, then  $\Delta l/l = \Delta f/f$ . Laser frequency fluctuations can give spurious strain signals whose amplitude depends on the difference in length between the measurement and reference arms. Since the two interferometers share the same laser source, these spurious wavelength fluctuations are coherent in the two interferometers and disappear in the difference between the two measured strains. This noise cancellation behaviour implies that signal-to-noise should be higher for measured deviatoric strain than for uniform horizontal expansion or contraction.

The instruments are characterized by very high sensitivity (picostrain level), wide frequency band (from d.c. up to hundreds of Hz), and large dynamic range, limited only by the capability of maintaining optical alignment.

### 3. Correction for local effects on measured strain

Although the interferometer measures strain directly, local distortions, such as cavity effects due to tunnel installation, surface topography, and inhomogeneities in elastic constants, can bias strain measurement significantly, even if do not add stochastic noise.

Siting effects can also produce coupling among the different strain components, so that measured strain is not equal to the large-scale Earth strain. Strain distortions can be estimated under the assumption that the scale of these effects is much smaller than the scale of the measured stress and strain perturbations (e. g. Park et al. 2008). For example, this assumption holds for observations of Earth tides. Cavity effects are expected to be small on both Gran Sasso interferometers, since they measure extension along the axis of two tunnels and the distance between the end-monuments and the tunnel end faces are more than one tunnel diameter. Topographic effects are expected to be small on BA, but as large as 20% to 40% on BC, since (as shown in Figure 1) BA is approximately parallel to the local trend of the Apennines mountain chain and BC is approximately perpendicular to it. For a general discussion of cavity and topographic effects, see e. g. Harrison (1976).

We estimate local effects using reference Earth tide strains, a  $xy$  coordinate system (with the  $x$ -axis directed along BC and the  $y$ -axis directed along BA) and a matrix representation of the relationship between instrument and remote strains (Hart et al., 1996). Local effects on the extension along BA ( $\epsilon_{BA}$ ) can be described by the three coupling coefficients  $\alpha_{BA}$ ,  $\beta_{BA}$ , and  $\gamma_{BA}$ :

$$\epsilon_{BA} = \alpha_{BA} \epsilon_{xx} + \beta_{BA} \epsilon_{yy} + \gamma_{BA} \epsilon_{xy}$$

and similarly for the extension along BC ( $\epsilon_{BC}$ ).

The six unknown coefficients describing local effects have been estimated following a three-step approach.

As a first step, we compute the amplitude factor and phase lag related to 16 tidal groups in the diurnal and semi-diurnal bands (Q1, O1, M1, P1, S1, K1,  $\Psi$ 1,  $\Phi$ 1, J1, OO1, 2N2, N2, M2, L2, S2, K2) for recorded BA and BC extensions since 2001 to 2008 (see Figures 5 and 6) corrected for air pressure and temperature effects (VAV03 code, Venedikov et al. 2005).

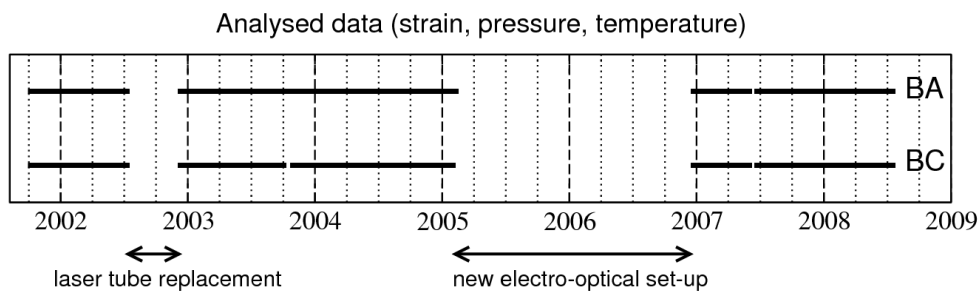


Figure 5. Records used to estimate coupling coefficients for the two interferometers.

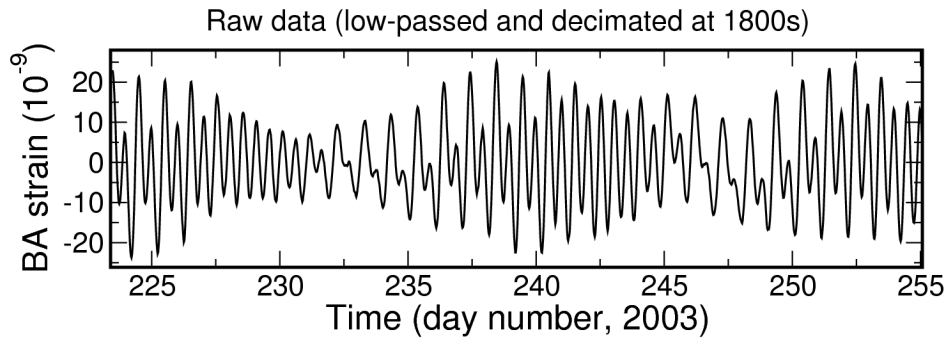


Figure 6. Example of strain data used for the tidal analysis.

As a second step, we compute theoretical (solid + ocean loading) strain tides for  $\epsilon_{xx}$ ,  $\epsilon_{yy}$ , and  $\epsilon_{xy}$ , using SPOTL (Agnew, 1997), Love numbers from IERS2003 (frequency-independent, but different in the diurnal and semi-diurnal bands; McCarthy and Petit, 2004), mass-loading Green functions for the Gutenberg-Bullen earth model A (Farrell, 1972), three different global ocean models (TPXO7.1, Egbert and Erofeeva, 2002; GOT00.2, Ray, 1999; CSR4.0, Eanes, 1994), and one local Mediterranean Sea model, at 1/30 deg resolution (four diurnal constituents, Q1, O1, P1, K1; four semi-diurnal constituents, N2, M2, S2, K2, <http://www.coas.oregonstate.edu/research/po/research/tide/med.html>). Tides in the Mediterranean Sea have small amplitude with respect to those in principal oceans, but contribute about half the total ocean loading strain at Gran Sasso, because of the dependence of ocean loading strain on distance. Global ocean models give very different and inaccurate representations of the Mediterranean Sea, and thus very different values of ocean loading strain at Gran Sasso. If the same local model is used for the Mediterranean Sea, all tested global models give very similar results (see Table 1 for K1 and M2). Since at Gran Sasso ocean loading tidal strain is smaller than solid Earth one by about an order of magnitude, total tidal strain predicted after merging the Mediterranean Sea model into different global models are practically undistinguishable (see Table 2 for K1 and M2).

We also check for differences in the results when varying the Earth model used for computing mass-loading Green functions. SPOTL distribution includes two variants of the Gutenberg-Bullen model A (referred to as gbavap), obtained after replacing top 1000 km by the continental shield crust and mantle structure of Harkrider (1970) (referred to as contap) and the oceanic crust and mantle structure of Harkrider (1970) (referred to as ocenap). Table 3 shows that total tidal strain at Gran Sasso is practically independent of the Earth model used for computing mass-loading Green functions.

Tidal constituent	Global ocean model	$\epsilon_{xx}$ Amplitude (n $\epsilon$ )	$\epsilon_{xx}$ Phase (deg)	$\epsilon_{yy}$ Amplitude (n $\epsilon$ )	$\epsilon_{yy}$ Phase (deg)	$\epsilon_{xy}$ Amplitude (n $\epsilon$ )	$\epsilon_{xy}$ Phase (deg)
K1	TPXO7.1	0.46	72.5	0.45	-64.2	0.29	70.2
K1	CSR4.0	0.46	73.3	0.45	-65.9	0.28	71.7
K1	GOT00.2	0.46	73.2	0.45	-63.7	0.29	71.0
M2	TPXO7.1	1.64	69.9	0.08	-68.8	1.84	-106.5
M2	CSR4.0	1.64	69.7	0.05	-61.3	1.87	-106.6
M2	GOT00.2	1.65	69.7	0.04	-36.6	1.86	-106.6

Table 1. Ocean loading strain at Gran Sasso, computed for the same local Mediterranean model merged into three different global models. The  $x$ -axis is directed along BC and the  $y$ -axis along BA, lags are negative.

Tidal constituent	Global ocean model	$\epsilon_{xx}$ Amplitude (n $\epsilon$ )	$\epsilon_{xx}$ Phase (deg)	$\epsilon_{yy}$ Amplitude (n $\epsilon$ )	$\epsilon_{yy}$ Phase (deg)	$\epsilon_{xy}$ Amplitude (n $\epsilon$ )	$\epsilon_{xy}$ Phase (deg)
K1	TPXO7.1	6.81	-14.0	9.33	10.3	2.19	-46.8
K1	CSR4.0	6.80	-14.0	9.32	10.3	2.19	-47.2
K1	GOT00.2	6.80	-14.0	9.34	10.3	2.19	-47.0
M2	TPXO7.1	12.09	23.3	5.41	-37.7	4.18	164.0
M2	CSR4.0	12.10	23.3	5.39	-37.4	4.18	164.4
M2	GOT00.2	12.10	23.3	5.39	-37.2	4.18	164.4

Table 2. Total tidal strain at Gran Sasso, computed for the same local Mediterranean model merged into three different global models. The  $x$ -axis is directed along BC and the  $y$ -axis along BA, lags are negative.

Tidal constituent	Earth model	$\epsilon_{xx}$ Amplitude (n $\epsilon$ )	$\epsilon_{xx}$ Phase (deg)	$\epsilon_{yy}$ Amplitude (n $\epsilon$ )	$\epsilon_{yy}$ Phase (deg)	$\epsilon_{xy}$ Amplitude (n $\epsilon$ )	$\epsilon_{xy}$ Phase (deg)
K1	gbavap	6.80	-14.0	9.32	10.3	2.19	-47.2
K1	contap	6.80	-13.8	9.31	11.0	2.21	-47.3
K1	ocenap	6.81	-14.1	9.33	11.0	2.22	-47.9
M2	gbavap	12.10	23.3	5.39	-37.4	4.18	164.4
M2	contap	12.11	23.0	5.37	-37.0	4.16	164.7
M2	ocenap	12.05	22.8	5.43	-37.9	4.20	163.1

Table 3. Total tidal strain at Gran Sasso, computed for the local Mediterranean model merged into the CSR4.0 global model, and three different Earth models (see text). The  $x$ -axis is directed along BC and the  $y$ -axis along BA, lags are negative.

The phasor plot in Figure 7 shows ocean loading correction to theoretical solid tides (computed for a spherical non-rotating Earth, SNRE) for the two interferometers. Correction essentially consists in a small rotation of phasors, whose amount and sign depends on the tidal component and the interferometer.

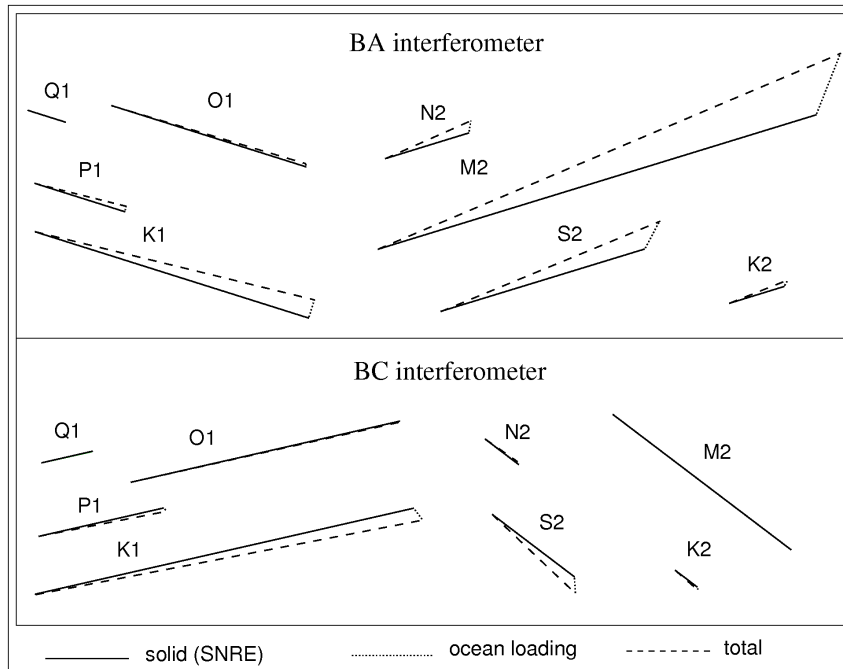


Figure 7. Phasor plot of predicted solid (solid lines), ocean loading (dotted lines), and total (dashed lines) tidal strain. Ocean model: TPXO7.1 and local Mediterranean model; Earth model for mass-loading Green functions: Gutenberg-Bullen model A; Love numbers: IERS 2003.

We assume that discrepancies between tidal predictions and observations out of the Free Core Resonance spectral region are only due to local effects (heterogeneities, topography, etc.). Thus, as a third step, we use a least-square fitting technique to estimate the coupling coefficients for BA and BC by comparing predicted and observed amplitudes and phases of the larger tides out of the Free Core Resonance range, namely Q1, O1, N2, M2, and K2. We do not use S2 because of possible residual contamination from air pressure effects. The fit thus involves ten equations (five cosine and five sine amplitudes) and three unknowns ( $\alpha$ ,  $\beta$ ,  $\gamma$ ) for each interferometer. The goodness of the fit gives an indication of the acceptability of the assumptions (capability of modelling discrepancies between tidal predictions and observations through the coupling matrix) because the problem is overdetermined. The phasor plot in Figure 8 clearly shows that discrepancies are fully recovered by using the coupling matrix (dashed and dotted lines are indistinguishable), which in case we use the

TPXO7.1 ocean model, the local Mediterranean model, the Gutenberg-Bullen model A for mass-loading Green functions, and the IERS 2003 Love numbers, is given by

$$\varepsilon_{BA} = -0.009 \varepsilon_{xx} + 0.927 \varepsilon_{yy} + 0.187 \varepsilon_{xy}$$

$$\varepsilon_{BC} = 0.702 \varepsilon_{xx} - 0.011 \varepsilon_{yy} + 0.053 \varepsilon_{xy}$$

Coupling coefficients obtained using different Earth and ocean models are very similar (even if not identical) to those shown here. Since strain noise is red, i. e. power spectral density increases with diminishing frequencies, we also perform the same three-step analysis using first-differenced strain time series to deal with white noise (e. g. Amoruso et al., 2000) obtaining again very similar results. Coupling among different strain components is faint but, as expected, strain measured along BC is reduced by about 30% because of topographic effects.

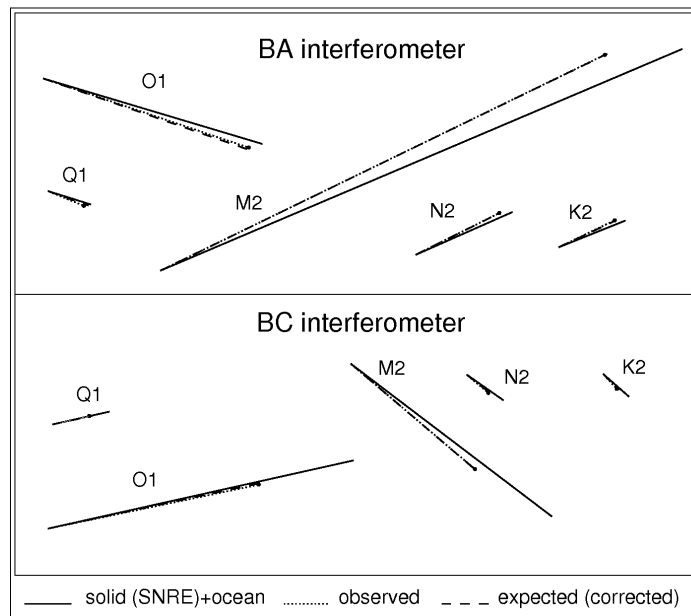


Figure 8. Phasor plot of predicted total (solid lines), observed (dotted lines), and corrected (through the coupling matrix, dashed lines) tidal strain. Ocean model: TPXO7.1 and local Mediterranean model; Earth model for mass-loading Green functions: Gutenberg-Bullen model A; Love numbers: IERS 2003.

## Conclusions

In their previous configuration, the laser interferometers at Gran Sasso already produced interesting results as regards slow earthquakes (Crescentini et al. 1999; Amoruso et al., 2002) and free oscillations of the Earth (Park et al. 2008). However, their electro-optical set-up has been recently modified with respect to the original version to reduce costs and improve reliability. Output of each interferometer now consists of two quadrature signals, whose Lissajous figure is inverted for

changes in length of the 90-m-long baselines. Two-year data recorded with the new configuration show that changes did not degrade instrumental performances.

Even if these top-rank instruments give high-quality strain data, siting effects produce coupling among the different strain components, so that measured strain is not equal to the large-scale Earth strain. We estimate local effects using reference tidal strains and a matrix representation of the relationship between instrument and remote strains. The three coupling coefficient of each interferometer (obtained by best-fitting) are able to make differences between observed and predicted tides negligibly small. Also negligible is the dependence of numerical values of the coefficients on the Earth and ocean models used to compute theoretical total tides.

### Acknowledgments

This research has benefited from funding provided by the Istituto Nazionale di Geofisica e Vulcanologia. We are grateful to the Laboratori Nazionali del Gran Sasso – INFN for logistic support.

### References

- Agnew, D. C., 1986. Strainmeters and Tiltmeters, *Rev. Geophys.*, 24(3), 579-624.
- Agnew, D. C., 1997. NLOADF: a program for computing ocean-tide loading, *J. Geophys. Res.*, 102, 5109-5110.
- Amoruso, A., and Crescentini, L., 2008. Free Core Resonance parameters from strain data: results from the Gran Sasso (Italy) extensometers, *New Challenges in Earth's Dynamics*, ETS 2008, 1<sup>st</sup>-5<sup>th</sup> September 2008, Jena, Germany.
- Amoruso, A., Crescentini, L., Scarpa, R., 2000. Removing tidal and atmospheric effects from Earth deformation measurements. *Geophys. J. Int.*, 140, 493-499.
- Amoruso, A., Crescentini, L., Morelli, A., Scarpa, R., 2002. Slow rupture of an aseismic fault in a seismogenic region of Central Italy, *Geophys. Res. Lett.*, 29(24), 2219.
- Buklarskii, A. V., Kart, A. M., Klyachko, B. S., Kravchuk, V. K., Milyukov, V. K., Melezhnikov, I. V., Myasnikov, A. V., Nesterov, V. V., and Rudenko, V. N., 1995. Baksan laser interferometer, *Measurement Techniques*, 38, 1073-1081.
- Crescentini, L., Renzella, G., 1991. A wide-band high-sensitivity laser strainmeter. *Rev. Sci. Instrum.*, 62, 1206-1209.
- Crescentini, L., Amoruso, A., 1996. Improving the SOPRA DMDP2000 spectrometer by a Michelson interferometer. *Rev. Sci. Instrum.*, 67, 3044-3046.
- Crescentini, L., Amoruso, A., Fiocco, G., and Visconti, G., 1997. Installation of a high-sensitivity laser strainmeter in a tunnel in central Italy, *Rev. Sci. Instrum.*, 68, 3206-3210.
- Crescentini, L., Amoruso, A., and Scarpa, R., 1999. Constraints on Slow Earthquake Dynamics from a Swarm in Central Italy, *Science*, 286, 2132.

- Eanes, R. J., 1994. Diurnal and semidiurnal tides from TOPEX/POSEIDON altimetry. *Eos Trans. AGU*, 75(16), 108.
- Egbert, G. D., Erofeeva, S. Y., 2002. Efficient inverse modeling of barotropic ocean tides. *J. Atmos. Oceanic Technol.*, 19, 2, 183-204.
- Farrell, W. E., 1972. Deformation of the Earth by surface loads, *Rev. Geophys and Space Phys.*, 10, 761-797.
- Gouly, N. R., King, G. C. P. and Wallard, A. J., 1974. Iodine stabilized laser strainmeter, *Geophys. J. R. Astron. Soc.*, 39, 269-282.
- Harkrider, D., 1970. Surface waves in multilayered elastic media (2): higher mode spectra and spectral ratios from point sources in plane-layered earth models. *Bull. Seismo. Soc. Amer.*, 60, 1937.
- Harrison, J. C., 1976. Cavity and Topographic effects in tilt and strain measurements. *J. Geophys. Res.*, 81, 319-328.
- Hart, R. H. G., Gladwin, M. T., Gwyther, R. L., Agnew, Wyatt, F. K., 1996. Tidal calibration of borehole strain meters: Removing the effects of small-scale inhomogeneity. *J. Geophys. Res.*, 101, 25553-25571.
- Levine, J., Hall, J. L., 1972. Design and Operation of a Methane Absorption Stabilized Laser Strainmeter. *J. Geophys. Res.*, 77, 2595-2609.
- McCarthy, D. D., Petit, G. (eds.), 2004. IERS Conventions (2003), IERS Technical Note No. 32.
- Mukai, A., Takemoto, S., Yamamoto, T., 2004. Fluid core resonance revealed from a laser extensometer at the Rokko-Takao station, Kobe, Japan. *Geophys. J. Int.*, 156, 22-28.
- Park, J., Amoruso, A., Crescentini, L., Boschi, E., 2008. Long-period toroidal earth free oscillations from the great Sumatra–Andaman earthquake observed by paired laser extensometers in Gran Sasso, Italy. *Geophys. J. Int.*, 173, 887-905.
- Ray, R. D., 1999. A Global Ocean Tide Model From TOPEX/POSEIDON Altimetry: GOT99.2. NASA Technical Memorandum 209478.
- Sacks, I. S., Snoke, J. A., Evans, R., King, G., Beavan, J., 1976. Single-site phase velocity measurement. *Geophys. J. R. Astr. Soc.*, 46, 253-258.
- Takemoto, S., Araya, A., Akamatsu, J., Morii, W., Momose, H., Ohashi, M., Higashi, T., Fukuda, Y., Miyoki, S., Uchiyama, T., Tatsumi, D., Hanada, H., Naito, I., Telada, S., Ichikawa, N., Onoue, K., Wada, Y., 2004. A 100 m laser strainmeter system installed in a 1 km deep tunnel at Kamioka, Gifu, Japan. *J. Geodyn.*, 38, 477-488.
- Venedikov, A. P., Arnosó, J., Vieira, R., 2005. New version of program VAV for tidal data processing. *Computers & Geosciences*, 31, 667-669.